

Journal of Materials Chemistry B

Accepted Manuscript



This is an *Accepted Manuscript*, which has been through the Royal Society of Chemistry peer review process and has been accepted for publication.

Accepted Manuscripts are published online shortly after acceptance, before technical editing, formatting and proof reading. Using this free service, authors can make their results available to the community, in citable form, before we publish the edited article. We will replace this *Accepted Manuscript* with the edited and formatted *Advance Article* as soon as it is available.

You can find more information about *Accepted Manuscripts* in the [Information for Authors](#).

Please note that technical editing may introduce minor changes to the text and/or graphics, which may alter content. The journal's standard [Terms & Conditions](#) and the [Ethical guidelines](#) still apply. In no event shall the Royal Society of Chemistry be held responsible for any errors or omissions in this *Accepted Manuscript* or any consequences arising from the use of any information it contains.

COMMUNICATION

pH-Responsive Hierarchical Transformation of Charged Lipid Assemblies within Polyelectrolyte Gel Layers with Applications for Controlled Drug Release and MR Imaging Contrast

Cite this: DOI: 10.1039/x0xx00000x

Received 00th January 2012,

Accepted 00th January 2012

DOI: 10.1039/x0xx00000x

www.rsc.org/

Yi-Fong Huang,^a Wen-Hsuan Chiang,^b Wen-Chia Huang,^b Hsin-Hung Chen,^a Ming-Yin Shen,^{b,c} Sung-Chyr Lin,^a Chorng-Shyan Chern,^d and Hsin-Cheng Chiu^{*b}

Cationic lipid-embedded poly(acrylic acid) (PAAc) gel layer coated on the chitosan/superparamagnetic iron oxide nanoparticle (SPION) nanohybrid surfaces effectively modulates drug release and MR imaging contrast by pH-responsive morphological transformation and hierarchical alignment of the lipid assemblies.

The great potential of nanoscale delivery systems of bioactive agents for cancer therapeutics and diagnostics demonstrated in the past decade comes mostly from the feasibility of imparting pertinent stimuli-responsive properties to the systems and the local accumulation of nanoparticles within tumor.¹⁻⁴ While the latter is intimately associated with the facilitated extravasation and enhanced residence of nanoscale structures within tumor tissue (i.e., the enhanced permeability and retention effect), the former enhances the therapeutic/diagnostic performance in a well controlled manner. This is mainly achieved via the delicate design in structural/morphologic response to external or internal stimuli. Polymeric assemblies (e.g., micelles and vesicles) from intermolecular packing of block or graft amphiphilic copolymers have been one of primary interests in the nanomedicine applications owing to their controllable responses in supramolecular architectures to environmental stimuli.⁵⁻¹⁰ Taking advantage of the structural response to external stimuli (e.g., temperature, pH, light and voltage), polymeric vehicles could achieve selective delivery/release of small drugs, proteins, genes and diagnostic probes.⁵⁻¹⁰ For example, pH-responsive micelles from assembly of the block copolymer of poly(ethylene glycol) (PEG) and cholic acid-conjugated poly(N-(N',N'-diisopropylaminoethyl) aspartamide) (PAsp(DIP)) in aqueous solution of pH 7.4 were developed for co-delivery of paclitaxel molecules and quantum dots to tumor tissues.⁵ Through the acid-induced protonation and

dissolution of PAsp(DIP) interlayer at low pH, drug species were released promptly. The voltage-responsive vesicles could be attained from orthogonal assembly of poly(styrene)- β -cyclodextrin and PEG-ferrocene in aqueous solution via terminal host-guest interactions.⁸ The reversible association and disassociation of polymeric vesicles and the liberation of entrapped cargoes can be remotely controlled by alteration of applied voltage strength.

It should be noted that most copolymers used to fabricate stimuli-responsive polymeric assemblies require rather complicated chemical processes along with the use of toxic reagents and organic solvents, thereby severely limiting their practical applications in biomedical field. To address this issue, it is essential to design a facile and reproducible approach to prepare a drug delivery system comprising polymeric assemblies with desirable stimuli-responsive properties. In our previous work,¹¹ pH-responsive hybrid nanovesicles were readily obtained from spontaneous co-assembly of poly(acrylic acid) (PAAc)-g-monomethoxy poly(ethylene glycol) (mPEG) with a cationic lipid, didodecyltrimethylammonium bromide (DDAB), in aqueous solution of pH 8.9 via electrostatic interaction. With the solution pH being reduced to 5.0, unionized AAc-rich transmembrane channels were formed at locations near mPEG coronas because of the significant disruption of consecutive ionic pairings of DDAB species with PAAc segments in vesicle membrane by the aid of the presence of extremely hydrated and mobile mPEG chains extending into the aqueous phase. The greatly promoted release of the encapsulated therapeutic payload can then be achieved. In this work, the lipid-embedded polyelectrolyte gel surface layer (serving as a pH-controllable molecular valve-like device) surrounding a magnetic core particle was developed. This unique device was achieved simply by the morphologic transformation and hierarchical alignment of cationic lipid assemblies within the thin PAAc gel layer. 1,2-Dioleoyl-3-

trimethylammonium-propane (DOTAP) was used to demonstrate the lipid hierarchical assembly in response to changes in environmental pH in this study. Small angle X-ray scattering (SAXS) patterns showed that sphere-like DOTAP micelles inside the PAAc-constituting gel layer at pH 7.4 underwent morphologic transformation upon acid-triggered reduction in both ionization of AAc residues and charge binding with DOTAP species. This led to re-assembly of DOTAP species into rod-like structure (for example, at pH 6.0) and hierarchical packing into disk-like aggregates (at pH 5.4) (Figure 1). Concomitantly, due to the significant change of electrostatic interaction of DOTAP species in different assembly structures with the AAc residues of the gel layer, the cross-linking density of the gel layer varies, thereby leading to permeability regulation of the gel layer to water molecules as well as to the therapeutic payload.

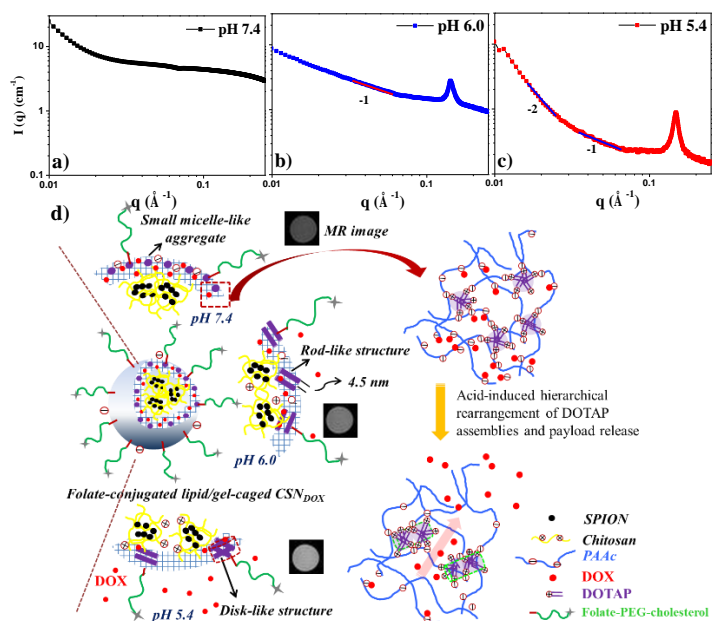


Figure 1. SAXS profiles of the lipid/gel-caged CSN in aqueous solution at a) pH 7.4, b) 6.0 and c) 5.4. d) Schematic illustration of the pH-triggered structural transition of DOTAP aggregates in the gel layer of the lipid/gel-caged CSN with controlled drug release and MR imaging contrast.

To demonstrate the capability of hierarchical lipid assembly structures in controlling the gel permeability, the cross-linked polyelectrolyte gel layer laden with both DOTAP and doxorubicin (DOX; an anticancer agent) was coated onto the organic/inorganic hybrid nanosphere. The template particles were prepared by coassembly of chitosan with citric acid-modified superparamagnetic iron oxide nanoparticles (SPION; ca. 8–10 nm in diameter, Figure S1a) via electrostatic interaction. To prevent the gel-coated particles from aggregation at low pH, they were further stabilized by ω -cholesterol-PEG-folate via the steric stabilization effect. Note that the cholesterol moiety was used as an anchor, and folate used as a targeting ligand in nanomedicine applications. The schematic representation of the particle morphology is illustrated in Figure 1. The preparation of citric acid-conjugated SPION, chitosan/SPION (CSN) templates, ω -cholesterol-PEG (Mw 2000 g/mol)-folate, DOTAP/DOX-laden gel-coated nanoparticles are described in detail in Supporting Information. The template particles have a mean hydrodynamic diameter (D_h) of ca. 70 nm and relatively uniform particle size distribution (polydispersity index (PDI) 0.21) (Table 1). Distinct from the zeta potential of the citric acid-covered SPION

alone (-24 mV at pH 5.0), the zeta potential of CSN was changed from -24 to +35 mV. This confirms the formation of hybrid complexes surrounded by positively charged chitosan chain segments for the template particles. After being caged with the PAAc gel layer at pH 6.0, the particles were enlarged to ca. 91 nm. They further grew to 120 nm after drug loading at pH 7.4. With cationic DOTAP species being embedded, the particle size became rather invariant in response to changes in pH, yet the surface charge density, as reflected in the zeta potential data, remained strongly pH dependent (Table 1 and Figure S5). It is also interesting to note that the polyelectrolyte gel can endow CSN with a more robust structure to resist the large-volume dilution with phosphate buffered saline (PBS) (Figure S6). TEM images of gel-caged nanoparticles clearly illustrate the spherical morphology and verify the successful deposition of PAAc-based gel onto the template particle surface (Figure S1b and c).

Table 1. Mean hydrodynamic diameters (D_h), polydispersity indices (PDI) and zeta potential values of hybrid nanoassemblies in aqueous solutions at 25 °C.

Sample	pH	D_h (nm)	PDI	ζ -potential (mV)
CSN	5.0	70 ± 4	0.21	35 ± 2
Gel-caged CSN	6.0	91 ± 3	0.15	-36 ± 3
	7.4	101 ± 4	0.17	-46 ± 2
Lipid/gel-caged CSN	7.4	120 ± 3	0.16	-39 ± 4
	5.4	123 ± 3	0.16	-24 ± 4
Lipid/gel-caged CSN _{DOX}	7.4	120 ± 4	0.15	-39 ± 2
FA-conjugated lipid/gel-caged CSN _{DOX}	7.4	119 ± 3	0.17	-20 ± 2

Through simple incorporation of DOTAP species with a preset weight ratio (e.g., $W_{\text{DOTAP}}/W_{\text{PAAc}} = 0.25$ (w/w)) into the aqueous gel-caged CSN dispersion at pH 7.4, lipid assemblies were readily developed within the PAAc-constituting outlayered gel phase. The resultant particles showed an appreciable increase in particle size and a slight reduction in zeta potential, yet retained a mono-modal particle size distribution (Table 1 and Figure S5). The TEM image also verifies the essentially unchanged particle morphology after incorporating DOTAP into the gel layer (Figure S1d). Obviously, DOTAP species became mostly embedded inside the gel layer that thus enlarged the surface layer dimension. At pH 7.4, at which the AAc residues were mostly deprotonated, the amphiphilic DOTAP molecules within the gel layer underwent hydrophobically-driven assembly via their nonpolar tails while the positively charged head groups being associated with the ionized AAc residues via electrostatic interaction. The pH-evolved variation of the interaction of DOTAP molecules with ionized AAc residues and the subsequent structural rearrangement of DOTAP assembly and the potential applications in nanomedicine are the major foci to be explored in this study.

The effects of medium pH on the primary molecular packing architecture of DOTAP species and the secondary assembly alignment within the gel surface layer surrounding CSN template were studied mainly by SAXS. As revealed in Figure 1a, the scattering profile of lipid/gel-coated CSN at pH 7.4 shows the absence of any characteristic Bragg peaks. Considering such a high level of lipid being accommodated within the gel layer, it is most likely that the resultant lipid assembly exhibits a spherical micelle-like structure (ca. 3.2 nm in radius as estimated by spherical micelle modeling fit) characterized by the lack of regular lamellae arrangement, as evidenced by SAXS measurements. Nonpolar tails

of DOTAP species self-associate with one another to form the hydrophobic core. In the meantime, the cationic head groups located within the micellar shell electrostatically interact with the ionized AAc units of the gel phase. As a result, lipid micelles reside randomly throughout the gel layer and act as additional effective cross-linking junctions by connecting themselves with PAAc chain segments via the charge interaction. This will then lead to an increase in the cross-linking density of the gel phase. The schematic illustration of lipid micelles acting as the cross-linking points within the nanogel layer is shown in Figure 1d.

When the medium pH is lowered from 7.4 to 6.0, the SAXS profile of the lipid/gel-caged CSN exhibits a sharp Bragg peak with an interlamellar d spacing ($2\pi/q$) of ca. 4.5 nm at $q = 0.14 \text{ \AA}^{-1}$. The scattering intensity decay perfectly matches the power law dependence of q^{-1} ($\alpha = 1$) in the q region $0.03\text{--}0.06 \text{ \AA}^{-1}$. This strongly suggests the development of rod-like DOTAP micelles (with ca. 3.9 nm and 9.1 nm in radius and length, based on cylinder modeling fit), which closely align to each other with a d spacing of 4.5 nm (Figure 1b). Similar SAXS observations on rod-like micelle structure in simple aqueous phases have been reported elsewhere.^{12–14} This is primarily due to the reduced negative charges within the gel layer and, consequently, the decreased electrostatic interaction of the AAc residues with DOTAP species. Under the circumstances, the morphologic transformation of DOTAP micelles into rod-like structure and inter-assembly alignment occurs. With the medium pH being further reduced to 5.4, the SAXS profile was well fitted to the power law dependence of q^{-1} in higher q range ($0.03\text{--}0.06 \text{ \AA}^{-1}$) and q^{-2} in the lower range ($0.012\text{--}0.025 \text{ \AA}^{-1}$), respectively (Figure 1c). Such a scattering pattern illustrates the formation of disk-like lipid aggregates within the AAc-rich gel layer, which is in line with the single particle form factor ($\alpha = 2$) of a disk in the low q region.^{12,15,16} According to the q^{-1} dependence in the q range $0.03\text{--}0.06 \text{ \AA}^{-1}$, the plate structure formed primarily by enhanced stacking of primary rod-like lipid assemblies into such a secondary-level architecture. Such a hierarchical alignment also resulted in a slight reduction in d -spacing from 4.5 to 4.2 nm. In view of the absence of morphologic response of DOTAP assemblies dispersed in water to changes in pH (data not shown), the pH-evolved morphologic transformation from spherical to rod-like structure and subsequent hierarchical alignment of the primary rod-like structure into the secondary plate structure are controlled virtually by the degree of ionization of the AAc residues and charge binding of the AAc units with DOTAP species in the gel layer (Figure 1d). This inevitably leads to an increase in the size of individual DOTAP aggregates and a decrease in the extent of physical cross-links.

Figure 2a shows that, in the absence of DOTAP, the cumulative release of DOX from gel-coated CSN is rather fast and uncontrollable, more than 80% over a period of 12 h at either pH 7.4 or 5.4 ($I = 0.15 \text{ M}$). With DOTAP being embedded in the gel layer ($W_{\text{DOTAP}}/W_{\text{PAAc}} = 0.25 \text{ (w/w)}$), the drug unloading at pH 7.4 was largely retarded. Nevertheless, the response in drug release to changes in pH in the range 7.4~5.4 is significantly enlarged. Figure 2b shows the influence of the level of DOTAP incorporated into the gel layer on the drug release at pH 7.4 (or 5.4) over a period of 12 h. Note that the drug release ratio, defined as the ratio of the cumulative drug release at pH 5.4 to that at pH 7.4 over a period of 12 h, was used as a quantitative pH-responsive unloading index in this work. Although the drug release at pH 7.4 (or 5.4) decreases with increasing the level of DOTAP, the pH-responsive unloading index reaches a maximal value at the weight ratio ($W_{\text{DOTAP}}/W_{\text{PAAc}}$) of 0.25. Obviously, accommodation of DOTAP within the outlayered gel at such an optimal level can effectively prevent DOX from prematurely leaking at pH 7.4 while desirable drug unloading at mildly acidic pH can be achieved. Compared with the lipid-free

case, the pH-induced hierarchical rearrangement of DOTAP assemblies within the PAAc gel layer is obviously the root cause for the delicate regulation of DOX release (Figure 1d). At pH 7.4, the cross-linking density of the gel layer is greatly enhanced as a result of the presence of spherical micelles of DOTAP in large quantity, which serve as additional cross-link junctions. With the medium pH being reduced from 7.4 to 5.4, transformation of primary spherical assemblies of DOTAP to rod-like structure and subsequent hierarchical alignment of the rod-like structure into the secondary plate architecture occur in the gel layer. Thus, the cross-linking density of the gel layer is significantly reduced, which in turn facilitates drug efflux.

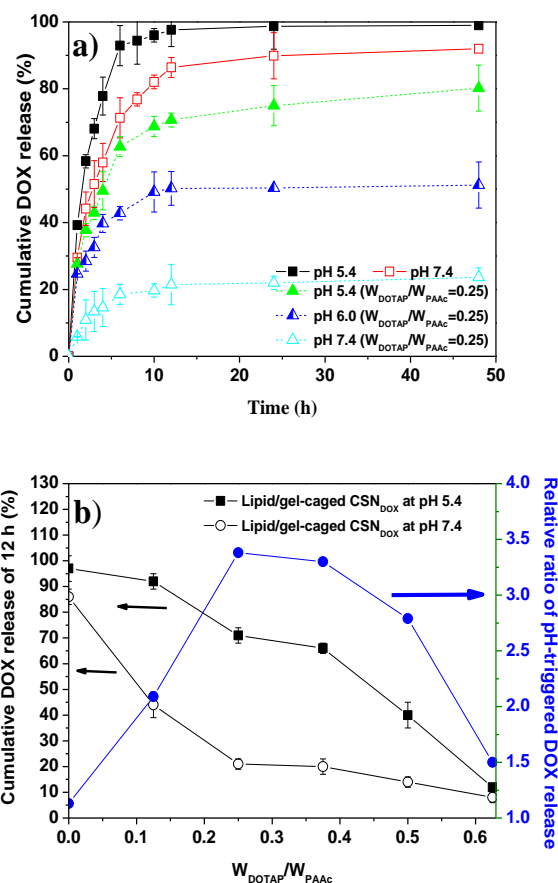


Figure 2. a) Time evolution of cumulative drug release for the gel-caged CSN_{DOX} (square) and lipid/gel-caged CSN_{DOX} (triangle) in aqueous solutions of different pH at 37 °C. b) Cumulative drug release of the lipid/gel-caged CSN_{DOX} with different weight ratios of DOTAP to PAAc ($W_{\text{DOTAP}}/W_{\text{PAAc}}$) at pH 5.4 and 7.4 over a period of 12 h. The profile of the ratio of the cumulative drug release at pH 5.4 to that at pH 7.4 as a function of $W_{\text{DOTAP}}/W_{\text{PAAc}}$ is also included.

SPION have been extensively exploited as a theranostic system in MR imaging, hyperthermia and magnetic guidance.^{17–20} Figure 3a shows that the lipid/gel-caged CSN at pH 5.4 exhibits an appreciably higher r_2 value as compared to either citric acid-coated SPION or CSN alone. The parameter r_2 is the slope of the straight line passing through the relaxation rate ($1/T_2$)-vs.-Fe concentration data points. Obviously, it is the high water-retaining capacity of the lipid-embedded gel layer surrounding CSN that is responsible for the enhanced MR imaging contrast. This is achieved by prolonging the acting time of water molecules in the CSN generated magnetic

field.^{21,22} With the pH being raised from 5.4 to 7.4, the r_2 value of the lipid/gel-coated CSN_{DOX} is considerably increased from 183 to 252 $\text{mM}^{-1}\text{s}^{-1}$ in contrast to the minor pH effect on r_2 for undecorated SPION. This is ascribed largely to the restrained spatial motion of the interior CSN, which is originating from the pH-evolved reinforcement of the cross-linking density of the gel layer in addition to the enhanced SPION clustering as a result of the reduced protonation of chitosan chain segments (Figure 1d). Again, the pH-triggered transformation and hierarchical alignment of lipid assemblies within the gel layer is the root cause. The pH-responsive T_2 -weighted MR imaging illustrated in Figure 3b is in well agreement with the observed r_2 values as a function of pH. Thus, the DOTAP-embedded polyelectrolyte gels show great potential to promote the pH-responsive MR imaging contrast and to be used to detect the pH of malignant tumoral microenvironments closely related to the resistance to cancer treatment and the mortal phenotype of cancer sickness.^{2,23,24} Additional in vitro evaluation of the entire folate (FA)-decorated lipid/gel-coated CSN_{DOX} as an effective theranostic delivery system was performed. The folate-decorated lipid/gel-caged CSN_{DOX} have been found capable to remarkably enhance intracellular DOX fluorescence intensity and T_2 -weighted MR image contrasts compared to the folate-free counterpart (Figure S8a). With the appreciable deposition of DOX species in cell nuclei (Figure S8b), the result also verifies effective drug release of the lipid/gel-coated CSN_{DOX} from acidic endosomes/lysosomes which is most likely achieved by the aid of the structural switch of lipid assemblies. More details are included in Electronic Supplementary Information.

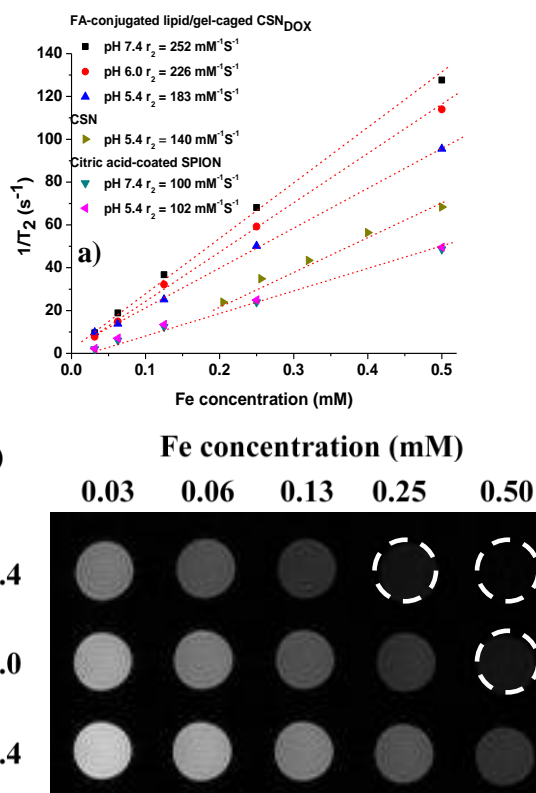


Figure 3. a) Reciprocal of T_2 (relaxation rate) as a function of Fe concentration for CSN at pH 5.4, folate-conjugated lipid/gel-caged CSN_{DOX} and citric acid-coated SPION at different pH. b) T_2 -weighted MR images of the folate-conjugated lipid/gel-caged CSN_{DOX} at different pH.

In summary, we have developed the outer PAAc-constituting gel layer, which is capable of modulating payload release and MR imaging contrast simply by embedding cationic DOTAP species within the gel layer. The DOTAP assemblies inside the gel layer undergo morphologic transformation from sphere to rod-like micelles and subsequent hierarchical alignment into disk-like stacking in response to regulated electrostatic interactions of DOTAP species with AAC residues when the medium pH changes from 7.4 to 5.4. Taking advantage of the structural switch of lipid assemblies as a control valve, the PAAc gel coated on CSN surface can greatly retard premature payload efflux at pH 7.4, yet retain satisfactory cargo release at pH 5.4. With the medium pH being adjusted, changes in both the gel structure and protonation of chitosan chain segments lead to a highly pH-controllable MRI contrast. This work demonstrates that combining the lipid-embedded polyelectrolyte gel surface layer with a magnetic core particle shows great potential to achieve effective cancer theranostics.

Acknowledgements

This work is supported by the National Science Council (NSC 102-2221-E-007-032-MY3 and NSC 102-2221-E-007-133-MY3), National Tsing Hua University (101N7046E1) and National Taiwan University Hospital-Hsinchu Branch (HCH103-036). The authors also thank the National Synchrotron Radiation Research Center (Hsinchu, Taiwan) for the use of SAXS (23A1) and 7T animal MRI Core Lab of the Neurobiology and Cognitive Science Center for technical and facility supports, and Instrumentation Center for MRI experiments at National Taiwan University.

Notes and references

^aDepartment of Chemical Engineering, National Chung Hsing University, Taichung 402, Taiwan.

^bDepartment of Biomedical Engineering and Environmental Sciences, National Tsing Hua University, Hsinchu 300, Taiwan.

^cDepartment of Surgery, National Taiwan University Hospital-Hsinchu Branch, Hsinchu 300, Taiwan

^dDepartment of Chemical Engineering, National Taiwan University of Science and Technology, Taipei 106, Taiwan

†Electronic Supplementary Information (ESI) available: Experimental details and further characterization of the folate-decorated lipid/gel-coated CSN_{DOX}. See DOI: 10.1039/c000000x/

- W. H. Chiang, V. T. Ho, W. C. Huang, Y. F. Huang, C. S. Chern and H. C. Chiu, *Langmuir*, 2012, **28**, 15056-15064.
- J. Y. Ko, S. Park, H. Lee, H. Koo, M. S. Kim, K. Choi, I. C. Kwon, S. Y. Jeong, K. Kim and D. S. Lee, *Small*, 2010, **6**, 2539-2544.
- S. M. Lee, Y. Song, B. J. Hong, K. W. MacRenaris, D. J. Mastarone, T. V. O'Halloran, T. J. Meade and S. T. Nguyen, *Angew. Chem., Int. Edit.*, 2010, **49**, 9960-9964.
- W. H. Chiang, W. C. Huang, C. W. Chang, M. Y. Shen, Z. F. Shih, Y. F. Huang, S. C. Lin and H. C. Chiu, *J. Control. Release*, 2013, **168**, 280-288.
- W. Wang, D. Cheng, F. M. Gong, X. M. Miao and X. T. Shuai, *Adv. Mater.*, 2012, **24**, 115-120.

6. Y. Li, G. H. Gao and D. S. Lee, *Adv. Healthc. Mater.*, 2013, **2**, 388-417.
7. W. Chen, F. H. Meng, R. Cheng and Z. Y. Zhong, *J. Control. Release*, 2010, **142**, 40-46.
8. Q. Yan, J. Y. Yuan, Z. N. Cai, Y. Xin, Y. Kang and Y. W. Yin, *J. Am. Chem. Soc.*, 2010, **132**, 9268-9270.
9. H. C. Chiu, Y. W. Lin, Y. F. Huang, C. K. Chuang and C. S. Chern, *Angew. Chem., Int. Edit.*, 2008, **47**, 1875-1878.
10. W. C. Huang, W. H. Chiang, S. J. Lin, Y. J. Lan, H. L. Chen, C. S. Chern and H. C. Chiu, *Adv. Funct. Mater.*, 2012, **22**, 2267-2275.
11. Y. F. Huang, W. H. Chiang, P. L. Tsai, C. S. Chern and H. C. Chiu, *Chem. Commun.*, 2011, **47**, 10978-10980.
12. S. Fujii, Y. Sanada, T. Nishimura, I. Akiba, K. Sakurai, N. Yagi and E. Mylonas, *Langmuir*, 2012, **28**, 3092-3101.
13. Y. L. Chiu, S. C. Chen, C. J. Su, C. W. Hsiao, Y. M. Chen, H. L. Chen and H. W. Sung, *Biomaterials*, 2009, **30**, 4877-4888.
14. I. Hoffmann, P. Heunemann, S. Prevost, R. Schweins, N. J. Wagner and M. Gradzielski, *Langmuir*, 2011, **27**, 4386-4396.
15. B. J. Heuser, M. M. C. Allain and W. C. Chen, *Phys. Rev. B*, 2002, **66**, 155419.
16. M. Kroon, W. L. Vos and G. H. Wegdam, *Int. J. Thermophys.*, 1998, **19**, 887-894.
17. A. J. Cole, V. C. Yang and A. E. David, *Trends Biotechnol.*, 2011, **29**, 323-332.
18. J. V. Jokerst and S. S. Gambhir, *Acc. Chem. Res.*, 2011, **44**, 1050-1060.
19. J. Xie and S. Jon, *Theranostics*, 2012, **2**, 122-124.
20. P. B. Santhosh and N. P. Ulrich, *Cancer Lett.*, 2013, **336**, 8-17.
21. C. Paquet, H. W. de Haan, D. M. Leek, H. Y. Lin, B. Xiang, G. Tian, A. Kell and B. Simard, *ACS Nano*, 2011, **5**, 3104-3112.
22. W. H. Chiang, V. T. Ho, H. H. Chen, W. C. Huang, Y. F. Huang, S. C. Lin, C. S. Chern and H. C. Chiu, *Langmuir*, 2013, **29**, 6434-6443.
23. K. E. Lokling, R. Skurtveit, A. Bjornerud and S. L. Fossheim, *Magnet. Reson. Med.*, 2004, **51**, 688-696.
24. D. Lindner and D. Raghavan, *Brit. J. Cancer*, 2009, **100**, 1287-1291.